Endothelial PKA targets ATG16L1 to regulate angiogenesis by limiting autophagy

Xiaocheng Zhao[1,2], Pavel Nedvetsky[1,2,3], Anne-Clemence Vion[4,5], Oliver Popp[6], Kerstin Zühlke[7], Gunnar Dittmar[6,8], Enno Klussmann[7,9], Holger Gerhardt[1,2,4,9,10]

[1] Vascular Patterning Laboratory, Center for Cancer Biology, VIB, Leuven, Belgium

[2] Vascular Patterning Laboratory, Center for Cancer Biology, Department of Oncology, KU Leuven, Leuven, Belgium

[3] Medical Cell Biology, Medical Clinic D, University Hospital Münster, Münster, Germany

[4] Integrative Vascular Biology Lab, Max-Delbrück Center for Molecular Medicine in the Helmholtz Association (MDC), Robert-Rössle-Strasse 10, Berlin 13125, Germany

[5]INSERM UMR-970, Paris Cardiovascular Research Center, Paris Descartes University, France

[6]Proteomics, Max-Delbrück Center for Molecular Medicine in the Helmholtz Association (MDC), Robert-Rössle-Strasse 10, Berlin 13125, Germany

[7]Anchored Signaling Lab, Max-Delbrück Center for Molecular Medicine in the Helmholtz Association (MDC), Robert-Rössle-Strasse 10, Berlin 13125, Germany

[8]LIH Luxembourg Institute of Health | CRP Santé · Department of Oncology

[9]DZHK (German Center for Cardiovascular Research), partner site Berlin

[10]Berlin Institute of Health (BIH), Berlin, Germany

Abstract

The cAMP-dependent protein kinase A (PKA) regulates a plethora of cellular functions in health and disease. During angiogenesis, PKA activity in endothelial cells controls the transition from sprouting to vessel maturation and limits tip cell formation independently of Notch signaling. The molecular PKA targets mediating these effects remain unknown. We report a chemical genetics screen identifying endothelial-specific substrates of PKA in human umbilical vein endothelial cells (HUVEC). We identified ATG16L1, a regulator of autophagy, as novel target of PKA. Biochemical validation, mass spectrometry and peptide spot arrays revealed that

PKA phosphorylates ATG16L1α at Ser268 and ATG16L1β at Ser269. The phosphorylations drive degradation of ATG16L1 protein. Knocking down PKA or inhibiting its activity increased ATG16L1 protein levels and endothelial autophagy. *In vivo* genetics and pharmacological experiments demonstrated that autophagy inhibition partially rescues vascular hypersprouting caused by PKA deficiency. We propose that endothelial PKA activity restricts active sprouting by reducing endothelial autophagy through phosphorylation of ATG16L1.

Introduction

Angiogenesis is the process of new blood vessels formation from pre-existing vessels via sprouting and remodeling. Blood vessels are crucial for tissue growth and physiology in vertebrates since they are the pipelines for oxygen and nutrients supply and for distribution of cells, such as of the immune system. Inadequate vessel formation and maintenance as well as abnormal vascular remodeling cause, accompany or aggravate many disease processes including myocardial infarction, stroke, cancer, and inflammatory disorders(Geudens & Gerhardt, 2011; Potente, Gerhardt, & Carmeliet, 2011).

Sprouting angiogenesis is a multistep process encompassing sprout initiation, elongation, anastomosis and final vascular network formation(Geudens & Gerhardt, 2011). Multiple molecular pathways have been identified to regulate sprouting angiogenesis; the most investigated are vascular endothelial growth factor (VEGF) and Notch/delta-like 4(DLL4) signalling. Whereas VEGF initiates angiogenesis through activating VEGF receptor 2 (VEGFR2), thereby guiding angiogenic sprouting and tip cell formation as well as stalk cell proliferation(Ferrara, Gerber, & LeCouter, 2003; Gerhardt et al., 2003), Notch and its ligand delta-like 4 (DLL4) limit tip cell formation and angiogenic sprouting(Hellström et al., 2007; Leslie et al., 2007; Lobov et al., 2007; Suchting et al., 2007). VEGF and Notch/DLL4 pathways co-operate to form a fine-tuned feedback loop to balance tip and stalk cells during developmental angiogenesis and to maintain vascular stabilization. In addition, PI3K/AktMAP4K4(Vitorino et al., 2015), ephrins and Eph receptors(Cheng, Brantley, & Chen, 2002), hedgehog signalling(Pola et al., 2001), YAP/TAZ(Kim et al., 2017; Neto et al., 2018), BMP signalling(Vion et al., 2018) and other pathways also regulate various aspects of angiogenesis.

Recently, we identified endothelial cAMP-dependent protein kinase A (PKA) as a critical regulator of angiogenesis during vascular development in vivo. Inhibition of endothelial PKA results in hypersprouting and increased numbers of tip cells, indicating that PKA regulates the transition from sprouting to quiescent vessels(Nedvetsky et al., 2016). However, the PKA targets mediating these effects remained unknown.

Here, we established a chemical genetics approach based on the mutation of a ‘‘gatekeeper residue’’ of the ATP-binding pocket of a protein kinase to identify endothelial-specific substrates of PKA. We verified autophagy-related-protein-16-like 1(ATG16L1) as a substrate of endothelial PKA and revealed that phosphorylation of ATG16L1 facilitates its degradation. *In vivo* experiments showed that autophagy inhibition partially rescued the hypersprouting and increased tip cell numbers caused by PKA deficiency.

Results

Screen for novel substrates of endothelial PKA

In order to identify direct substrates of endothelial PKA, we employed a chemical genetics approach(Allen, Lazerwith, & Shokat, 2005). The ATP-binding pocket of kinases contains a conserved “gatekeeper residue”, which in wild type (WT) kinases is usually a methionine or phenylalanine. Engineered analogue specific (AS) kinases replace this “gatekeeper residue” with a smaller amino acid (glycine or alanine), enabling the AS-kinases to accept ATP analogues (or ATPγS analogues) that are modified at the N^6 position with bulky groups as (thio-)phosphodonors. In contrast, WT-kinases poorly use these analogues. Once the substrates are thiophosphorylated by AS-kinases, they can be further alkylated and therefore recognized by a thiophosphate ester-specific antibody(Alaimo, Shogren-Knaak, & Shokat, 2001; Allen et al., 2007, 2005; Banko et al., 2011). To generate AS-PKACα, we mutated the methionine 120 to a glycine residue. Testing seven different variants of N^6-substituted bulky ATPγS analogues, we identified 6-cHe-ATPγS as the best thiophosphodonor for AS-PKACα substrates in HUVEC lysates (Figure S1).

To identify endothelial substrates of PKACα, HUVECs expressing WT-PKACα or AS-PKACα were lysed in kinase lysis buffer(KLB) and the thiophosphorylation reaction with 6-cHe-ATPγS was performed. After alkylation with p-Nitrobenzyl mesylate (PNBM), thiophosphorylated proteins were immunoprecipitation with rProtein G

Agarose beads coupled to the thioP antibody (Figure 1A). For quality control, one thirtieth of the protein on agarose beads was eluted for Western blot analysis, and the same amount was used for gel silver staining (Figure 1B). The rest was subjected to mass spectrometry analysis. Two independent experiments were performed. Candidate endothelial PKA targets were identified as peptides that were at least 2-fold (log ratio(AS/WT)>1) enriched in the AS-PKACα samples compared to WT- PKACα samples in both experiments.

The ninety-seven proteins identified in both experiments (Table S1) included several known PKA substrates such as NFATC1(Niswender et al., 2002), VASP(Anton et al., 2014; Butt et al., 1994; Profirovic, Gorovoy, Niu, Pavlovic, & Voyno-Yasenetskaya, 2005), PRKAR2A and PRKAR2B(Manni, Mauban, Ward, & Bond, 2008) indicating that the chemical genetic screen was a feasible approach to identify PKA substrates. Thirty proteins with at least 8-fold enrichment (log ratio(AS/WT)>3) are listed according to their log ratio(AS/WT) value in Table 1, presenting the most likely direct substrates of PKA in this screen.

To validate novel candidate PKACα substrates, we overexpressed WT-PKACα or AS-PKACα together with flag- or GFP- tagged candidate proteins in 293T cells, and used the 6-cHe-ATPγS as thiophosphate donor to thiophosphorylate substrates in lysates as described above. Lysate immunoprecipitation was carried out with M2 anti-flag beads or anti-GFP antibody coupled agarose beads, and the immune complexes were probed by western blot using thiophosphate antibody. The known PKA substrate NFATC1 served as a positive control. Five selected new candidate proteins (PPP1R12C, ATG16L1α, DDX17, ANKRD40 and ATG5) out of ninety-seven proteins were tested; four of these five proteins were confirmed to be thiophosphorylated by AS-PKACα, indicating that they are indeed direct substrates of AS-PKACα (figure 1C). Only ATG5 was not thiophosphorylated by AS-PKACα in the validation of the screen (figure 1C). Bioinformatic analysis of ATG5 amino acids sequence also failed to identify a consensus PKA substrate motif (R-R/K-X-S/T;K/R-X_{1-2}-S/T)(Kennelly & Krebs, 1991). Since ATG5 directly binds to ATG16L1(Matsushita et al., 2007; Noboru Mizushima, Noda, & Ohsumi, 1999), it likely co-precipitated with ATG16L1 in our screen.

ATG5 and ATG16L1 are conserved core components of the autophagy process, and PKA activity has been shown to negatively regulate autophagy in S. cervisiae and mammalian cells through phosphorylation of ATG1/ULK1(Noboru Mizushima, 2010).

ATG16L1 however has not previously been identified as a PKA target, prompting us to further investigate this interaction and the potential regulatory role of PKA and autophagy in endothelial sprouting.

PKACα phosphorylates ATG16L1α at S268 and ATG16L1β at S269

To identify the PKACα phosphorylation sites in ATG16L1, we spot-synthesized 25-mer overlapping peptides that cover the entire ATG16L1 protein. The peptide array was subjected to an *in vitro* PKA phosphorylation assay. Three peptides of the ATG16L1α and 7 peptides of ATG16L1β were higher phosphorylated compared to the negative control (figure 2A). The common amino acid sequences included in the phosphorylated peptides predicted Ser268 in ATG16L1α and Ser269 as well as Ser287 in ATG16L1β as potential PKA phosphorylation sites (figure 2B). Indeed serine to alanine mutation S268A in ATG16L1α and S269A mutation in ATG16L1β resulted in a loss of AS-PKACα thiophosphorylation of these two ATG16L1 isoforms (figure 2C and 2D). Moreover, LC-MS/MS analysis demonstrated phosphorylation of ATG16L1α at S268 and of ATG16L1β at S269 (figure 2E and 2F). Of note, thiophosphorylation was converted to normal phosphorylation by 1% TFA acid-catalyzed hydrolysis during sample preparation for LC-MS/MS, thus identifying the target sites as phosphorylated, not thiophosphorylated (figure S2). Together, these results demonstrate that S268 and S269 are the PKACα phosphorylation sites of ATG16L1α and ATG16L1β, respectively.

PKACα regulates ATG16L1 by phosphorylation-dependent degradation

Phosphorylation is one of the most widespread types of post-translational modification, and is crucial for signal transduction(C. Manning, D.B. Whyte, R. Martinez, T. hunter, 2002; Hunter, 1995; Ubersax & Ferrell, 2007). Previous research demonstrated that phosphorylation can regulate protein degradation by controlling its stabilization(Bullen et al., 2016; Geng, Wittwer, Dittrich-Breiholz, Kracht, & Schmitz, 2009; Hwang, Lee, & Kwon, 2009). To determine whether phosphorylation of ATG16L1α by PKA regulates protein stability, we overexpressed ATG16L1α^{WT} and the mutant ATG16L1α^{S268A} in HUVECs. To activate PKA, HUVECs were treated with the PKA specific activator 6-Bnz-cAMP. Using cycloheximide (CHX) to prevent new protein synthesis allowed us to detect the degradation of ATG16L1α^{WT} and ATG16L1α^{S268A} over time. Western blot analysis showed that most of the

ATG16L1α^{WT} degraded after 12 hours, whereas ATG16L1α^{S268A} remained largely stable (Figure 3A-3C), suggesting that the phosphorylation of ATG16L1α at site Ser268 by PKA promotes degradation. For ATG16L1β, Ser269 phosphorylation exhibited a similar function (figure 3D-3F). In accordance, depleting PKACα in HUVECs by shRNA led to accumulation of ATG16L1 (figure 3G). Moreover, in endothelial cells isolated from dnPKA^{iEC} mice (Prkar1a$^{Tg/+}$ crossed with Cdh5-CreERT2 mice expressing tamoxifen inducible Cre recombinase under control of endothelial specific Cdh5 promotor), ATG16L1 protein was also increased compared to endothelial cells isolated from Cdh5-CreERT2 control mice (figure 3H). Taken together, these results indicate that PKACα regulates ATG16L1 by phosphorylation-dependent degradation.

Inhibition of autophagy partially normalizes the vascular phenotype caused by PKA-deficiency

ATG16L1 is an important component of the ATG16L1-ATG5-ATG12 protein complex, required for LC3 lipidation and autophagosome formation. Both LC3 lipidation and autophagosome formation represent essential steps in autophagy (Kuma, Mizushima, Ishihara, & Ohsumi, 2002; Levine & Kroemer, 2008; Matsushita et al., 2007; N. Mizushima, 2003; Noboru Mizushima et al., 1999). Accumulation of ATG16L1 upon PKA knock down resulted in increased levels of the positive autophagy marker LC3II whilst reducing the negative autophagy marker p62 in HUVECs (figure 3G). Since ATG16L1 protein levels in endothelial cells isolated from dnPKA mice were also increased, we hypothesized that increased autophagy in endothelial cells may contribute to the vascular phenotype in these mice. If so, inhibiting autophagy could potentially normalize vascular hypersprouting in dnPKA^{iEC} mice. To test this hypothesis, we treated both wild type and dnPKA^{iEC} mice with the autophagy inhibitor chloroquine (CQ), performed retinal staining for isolectin B4 (IB4, membrane staining) and the tip cell specific marker ESM1, and quantified the IB4 and ESM1 positive areas. No significant difference were observed between wild type mice treated with PBS or CQ on both the vascular plexus and tip cells. However, CQ treatment partially rescued both the hyperdense vascular plexus front and the increasing tip cells in dnPKA^{iEC} mice (figure 4A-4C, fgure S3A). To confirm the specificity of this rescue genetically, we crossed the ATG5 conditional knock out mice ATG5^{ECKO} (ATG5$^{flox/flox}$ mice crossed with Cdh5-CreERT2 mice) with dnPKA^{iEC}

mice. Retinal stainings demonstrated that ATG5 deletion in endothelial cells in vivo, which shuts down autophagy, partially normalizes the hypersprouting phenotype of dnPKA^{iEC} mice(figure 4D-4F, fgure S3B). Together these results suggest that PKA regulates the switch from sprouting to stabilization of nascent vascular plexuses by limiting endothelial autophagy levels via ATG16L1 degradation.

Discussion

Our chemical genetics screen and biochemical analysis identified ATG16L1 as novel target of PKA activity in endothelial cells. The combined results demonstrate that PKA activity inhibits autophagy in culture human vein endothelial cells (HUVEC) via the phosphorylation of ATG16L1, which accelerates its degradation. In cultured bovine aortic endothelial cells, induction of autophagy by overexpression of ATG5 has been shown to promote in vitro vascular tubulogenesis, whereas ATG5 silencing suppressed this morphogenic behaviour(Du et al., 2012). In mice, inhibition of autophagy by bafilomycin, or genetic beclin heterozygosity as well as ATG5 knockout impairs angiogenesis post myocardial infarction, whereas the angiogenic factor AGGF1 enhances therapeutic angiogenesis through JNK -mediated stimulation of endothelial autophagy(Lu et al., 2016). Angiogenesis during tissue regeneration in a burn wound model also relied on induction of endothelial autophagy, by driving AMPK/AKT/mTOR signaling (Liang et al., 2018), together suggesting that autophagy regulation may represent a critical determinant of the extent of vascular sprouting. The identification of ATG16L1 as a direct target of PKA therefore raises the hypothesis that the dramatic hypersprouting phenotype in dnPKA^{iEC} mouse retinas deficient in endothelial PKA activity may result from exuberant endothelial activation of autophagy. Both chemical inhibition of autophagy and genetic endothelial inactivation of ATG5 partially normalized the hypersprouting phenotype in dnPKA^{iEC} mice, suggesting that indeed the activation of autophagy in dnPKA^{iEC} mice contributes to vascular hypersprouting. However, the failure to fully normalize vascular patterning by autophagy inhibition indicates that additional PKA targets and mechanisms may be involved. Our mass spectrometry analysis identified a list of presumptive endothelial PKA substrates, which will potentially also be involved in angiogenesis. For example, we identified RAPGEF2 as a candidate target, deficiency of which causes embryonic lethality at E11.5 due to yolk sac

vascular defects(Satyanarayana et al., 2010), very similar the yolk sac phenotype in dnPKA^{iEC} embryos(Nedvetsky et al., 2016). Similarly the potential target Rock2 has a well known role in regulating endothelial functions in angiogenesis(Liu et al., 2018; Montalvo et al., 2013; Seto, Chang, Jenkins, Bensoussan, & Kiat, 2016; Shimizu et al., 2013). Further studies will need to validate all the listed targets and establish which of these exert critical endothelial functions, and under what conditions.

An alternative explanation for the partial rescue of the dnPKAiEC phenotype by inhibition of autophagy could lie in additional functions of ATG16L1 itself. Although ATG16L1 plays an essential role in autophagy, and is part of a larger protein complex ATG16L1-ATG5-ATG12 that is necessary for autophagy, ATG16L1 is also involved in the production of inflammatory cytokines IL-1β and IL-18 and exerts anti-inflammatory functions during intestinal inflammation (Cadwell et al., 2008; Diamanti et al., 2017; Saitoh et al., 2008; Sorbara et al., 2013). IL-1β promotes angiogenesis by activating VEGF production during tumor progression(Carmi et al., 2013; Voronov et al., 2003), while IL-18 suppresses angiogenesis in cancer(Cao, Farnebo, Kurimoto, & Cao, 1999; Xing et al., 2016; Yang, Chen, Lu, Li, & Lin, 2010). How ATG16L1 regulates angiogenesis through inflammatory cytokines and whether this regulation operates downstream of PKA activity in vivo requires further investigation.

Intriguingly, our rescue experiments show that in wild type mice, inhibition of autophagy has no significant effect on developmental retinal angiogenesis. This could indicate that autophagy in developmental angiogenesis, unlike in pathological angiogenesis and post-ischemic tissue responses, is not very active.

Although, to our knowledge, this is the first identification of ATG16L1 as a PKA target and the first indication that PKA regulates autophagy in endothelial cells, PKA has previously been identified as regulator of autophagy. For example, PKA reduces autophagy through phosphorylation of ATG13 in *Saccharomyces cerevisiae*(Hundsrucker et al., 2006), and through phosphorylation of LC3 in neurons(Cherra et al., 2010). In our research, ATG16L1 was identified as a novel direct PKA substrate in endothelial cells, but not ATG13 or LC3. Mechanistically, the phosphorylation of ATG16L1 by PKA accelerates its degradation, and consequently decreases autophagy levels in endothelial cells. The finding of different components of the autophagy pathway as targets of PKA identified in yeast and various vertebrate cell populations raises the intriguing possibility that although the principle regulatory logic of PKA in autophagy is conserved, different protein targets mediate

this effect in different cells or organisms. In addition, or alternatively, this regulation carries multiple levels of redundancy, and the individual studies simply identify the most prevalent targets within the respective cell types. The fact that also ATG16L1 comes in two splice variants that are both targeted by PKA in endothelial cells lends some strength to this idea.

ATG16L1 can itself be regulated by multiple phosphorylation events by distinct kinases, with opposing effects on protein stability and autophagy. ATG16L1 can be phosphorylated at Ser139 by CSNK2 and this phosphorylation enhances its interaction with the ATG12-ATG5 conjugate(Song et al., 2015). IKKα promotes ATG16L1 stabilization by phosphorylation at Ser278(Diamanti et al., 2017). In addition, phospho-Ser278 has similar functions as phospho-Thr300, since both phospho-mutants ATG16L1^{S278A} and ATG16L1^{T300A} accelerate ATG16L1 degradation by enhancing caspase 3 mediated ATG16L1 cleavage(Diamanti et al., 2017; Murthy et al., 2014). In contrast, our finding suggest that the PKA target sites Ser268 in ATG16L1α (or Ser269 in ATG16L1β) work in the opposite way of Ser278 and Thr300; ATG16L1α^{S268A} (and ATG16L1β^{S269A}) are more stable than ATG16L1^{WT}. Furthermore, PKA deficiency also stabilizes ATG16L1 in endothelial cells *in vivo* and *in vitro*. Taken together, it appears that the different phosphorylation sites of ATG16L1 play different roles in fine tuning protein stability under the influence of alternative upstream kinases, and thereby adapt autophagy levels. Given the increasing insights into the role of autophagy in cell and tissue homeostasis and in disease, it will be of great interest to investigate whether the newly identified regulation by PKA extends beyond developmental angiogenesis into pathomechanisms associated with endothelial dysfunction.

Finally, on a technical note, the chemical genetics approach developed by Shoktat and colleagues(Alaimo et al., 2001; Allen et al., 2007, 2005) has successfully been used in other cell types, but to our knowledge, this is the first report on direct endothelial PKA targets. Our initial attempts using published cell lysate conditions based on RIPA buffer however failed to identify differences in thiophosphorylation when comparing AS-PKA expressing cells to WT-PKA expressing cells. Our buffer optimization revealed that RIPA buffer limits the activity of PKA kinase, whereas our new kinase lysis buffer (see methods) allows effective substrate phosphorylation, thus giving rise to strong signals in AS-PKA samples. This optimization will hopefully

be valuable for researchers aiming to utilize this approach for additional chemical genetic kinase substrate screens in the future.

Materials and Methods

Cell culture

Human Umbilical Vein Endothelial Cells (HUVECs) were freshly isolated and cultured in Endothelial Cell Growth Medium (Ready-to-use) (Promocell), passage 3 to 5 were used for experiments. HEK293T cells were cultured in Dulbecco's Modified Eagle Medium (DMEM, Thermo Fisher) with 10% Fetal Bovine Serum (FBS, Thermo Fisher) and 50 U/ml penicillin and 50 mg/ml streptomycin (Thermo Fisher) in 5% CO_2 at 37 °C.

Plasmid Construction

Lentivirus vector pRRLsin.PPT.CMV.flag.MCS was generated by resctrictional cloning of a sequence coding flag-tag into the pRRLsin.PPT.CMV.MCS vector at XbaI and XmaI restriction sites. It was used to generate flag-tagged constructs. PKACa, ANKRD40 and ATG5 were amplified from total RNA extracted from HUVECs and cloned into the pRRLsin.PPT.CMV.flag.MCS vector. pECE-M2-PPP1R12A wt, EGFPC1-huNFATc1EE-WT, pDESTmycDDX17, pMRX-IP/SECFP-hATG16L1 were purchased from Addgene. pDESTmycDDX17, pMRX-IP/SECFP-hATG16L1 and subcloned to vector pRRLsin.PPT.CMV.flag.MCS. PKACaM120G, ATG16L1α S268A, ATG16L1β S269A, ATG16L1β S287A, ATG16L1β S269A& S287A were generated by site-directed mutagenesis using Q5® Site-Directed Mutagenesis Kit (NEB). pLKO.1-TRC cloning shRNA vector (addgene) was used to clone PKACa shRNA constructs targeting sequence: TAGATCTCACCAAGCGCTTTG and TCAAGGACAACTCAAACTTAT.

Lentivirus production and infection

For lentivirus production, HEK293T cells, seeded in 150 mm dishes, were transfected with flag-tagged constructs, psPAX2 and pMD2.G using X-tremeGENE HP (Roche) as transfection reagent. Medium was changed 12-16 hours after transfection. Lentivirus-containing medium was collected in 24-48 hours afterwards

and filtered through 0.45 filters. Lentivius titers were determined with Lenti-X™ p24 Rapid Titer Kit (Clontech). To infect HUVEC, lentivirus (MOI 20-50) and polybrene (final concentration 8μg/ml) was added to cells for 18-22hours, and then the cells were washed with PBS and replaced the medium with fresh EGM2.

Protein extraction and Western Blot

Cells were lysed in RIPA buffer contained protease inhibitor cocktail and PhosSTOP™ (Roche). Protein concentrations were measured by Pierce™ BCA Protein Assay Kit. Samples were further diluted with SDS-loading buffer and SDS-PAGE was performed using NuPAGE™ 4-12% Bis-Tris Protein Gels (Invitrogen). Proteins were tranferred to nitrocellulose membrane with iBlot 2 Dry Blotting System (Thermos Fisher) or to PVDF membranes by wet blotting. Membranes were blocked with 5% nonfat milk in TBST and primary antibodies were incubated overnight at 4°C or 1.5 hours at room temperature. HRP-conjugated secondary antibodies were diluted and incubated 1 hour at room temperature. SuperSignal West Pico Chemiluminescent Substrate(Thermos Fisher) was used for imaging. Following antibodies were used: rabbit anti-thiophosphate ester (ab92570,1:5000) was from Abcam, goat anti-β-actin (sc-1615,1:2000) antibody, chicken anti-goat IgG-HRP (sc-516086,1:5000) were from Santa Cruz Biotechnology, rabbit anti-GAPDH (#2118,1:1000), rabbit anti-PKACa (#4782,1:1000), rabbit anti-ATG16L1 (#8089,1:1000), rabbit anti-p62 (#8025,1:1000), rabbit anti-LC3 (#3868,1:1000) antibodies and anti-rabbit IgG, HRP-linked antibody (#7074,1:2000) were from Cell Signaling, rabbit anti-flag (F7425,1:1000) and mouse anti-flag (F3165,1:1000) were from Sigma and rabbit anti-GFP (A11122,1:1000) was from Invitrogen. Peroxidase affinipure donkey anti-mouse IgG (715-035-151,1:2000) was from Jackson Immuno Research.

Chemical Genetic Screen and validation of PKA substrates

HUVECs (6 10cm-dishes each containing $1x10^6$ cells) were infected with lentivirus encoding either flag-PKACa WT (as negative control) or flag-PKACa M120G. 48 hours after infection, cells were stimulated with Sp-8-CPT-cAMPS (Biolog) for 10 minutes, then lysed in kinase lysis buffer (1% NP40, 142 mM NaCl, 25 mM Tris-HCl (pH 7.5), 5 mM β-glycerophosphate, 2 mM dithiothreitol, 0.1 mM Na_3VO_4, 10 mM

MgCl2) with protease inhibitor cocktail on ice for 20 minutes and spun (16,000g x 10min) to remove cell debries. 3.5 mM GTP and 350 μM 6-cHe-ATPγS (Biolog) were added to the lysates. After 30 min incubation at 30°C, 2.5 mM p-Nitrobenzyl mesylate (PNBM, Abcam) was added and the reaction was incubated for additional 2 hours at room temperature. PNBM was removed by Zeba™ Spin Desalting Columns, 7K MWCO (Thermo Fisher) and samples were washed with IP buffer (1% NP40, 150 mM NaCl, 50 mM Tris-HCl (pH 7.5), 0.5% sodium deoxycholate). The protein fractions were precleared by incubation with Recombinant Protein G Agarose for one hour at 4°C. The precleared samples were then incubated with anti-thiophosphate ester antibody (51-8; Abcam) coupled to Recombinant Protein G Agarose coupled gently rocking overnight at 4°C. The agarose beads were washed 4 times with IP buffer. 1/30 of the washed beads was boiled in SDS sample loading buffer for western blot detection or silver staining. The rest samples were used for mass spectrometry analyze.

For validation of the identified substrates, 293T cells ($1.5x10^6$ on a 6cm dish) were transfected with 0.5μg pRRL PKACa WT or pRRL PKACaM120G and 1.5 μg of indicated candidate substrate using X-tremeGENE HP DNA transfection reagent (Roche). 30 hours after transfection, cells were stimulated with Sp-8-CPT-cAMPS (Biolog) for 10 minutes, lysated and treated as described above.

Silver staining

Silver staining was performed using Pierce™ Silver Stain Kit (Thermo Fisher,24600) according to the manufacturer's protocol. Briefly, the SDS-page gel was washed in ultrapure water and fixed by fixing solution(30% ethanol,10% acetic acid) for 30 minutes. After incubating the gel in sensitizer working solution(provided in the kit) for 1 minutes, silver stain enhancer(provided in the kit) was added for another 5 minutes. Subsequently, the gel was incubated with developer working solution(provided in the kit) for 2-3 minutes, before stopping the reaction with stop solution(provided in the kit).

Mass spectrometry to identify new PKA substrates and phosphorylation sites

For mass spectrometric analysis to identify new PKA substrates, samples were prepared by chemical genetical approach as described above, each sample was run

on a stacking SDS-PAGE collecting all proteins in a single band. After coomassie blue staining, the minced gel pieces were digested with trypsin based on Shevchenko et al. (Shevchenko, Tomas, Havliš, Olsen, & Mann, 2007) in an automated fashion using a PAL robot (Axel Semrau / CTC Analytics). Samples were measured on an LTQ Orbitrap VELOS mass spectrometer (Thermo) connected to a Proxeon nano-LC system (Thermo). Five microliters of the sample was loaded on a nano-LC column (0.074 x 250 mm, 3 mm Reprosil C18; Dr. Maisch) and separated on a 155 min gradient (4%–76% acetonitrile) at a flow rate of 0.25 ml/min and ionized using a Proxeon ion source. Mass spectrometric acquisition was done at a resolution of 60,000 with a scan range of 200-1,700 m/z in FTMS mode selecting the top 20 peaks for collision-induced dissociation fragmentation. Tandem mass spectrometric scans were measured in ion-trap mode with an isolation width of 2 m/z and a normalized collision energy of 40. Dynamic exclusion was set to 60 s. For data analysis, the MaxQuant software package version 1.5.2.8(Cox & Mann, 2008) was used. Carbamidomethylation on cysteine was set as a fixed modification and oxidized methionine, acetylated N-termini and phosphorylation as variable modifications. An FDR of 0.01 was applied for peptides and proteins and the Andromeda search(Cox et al., 2011) was performed using a mouse Uniprot database (August 2014). MS intensities were normalized by the MaxLFQ algorithm implemented in MaxQuant(Cox et al., 2014). MaxLFQ-normalized intensities among the replicates of the groups to be related were used for comparison. For downstream analysis *R* was used to calculate fold changes and t-statistics.

For mass spectrometric analysis to identify phosphorylatin sites of ATG16L1, purified thiophosphorylated ATG16L1 proteins on beads were washed 3 times with 800 µl IP buffer followed by 3 times washing with 800 µl digestion buffer (20 mM Tris pH 8.0, 2 mM CaCl2) and dried. The washed beads were resuspended in 150 µl digestion buffer and incubated for 4 hours with 1 µg trypsin (Promega, catnr: V5111) at 37˚C. Beads were removed, another 1 µg of trypsin was added and proteins were further digested overnight at 37˚C. Peptides were acidified with 1% TFA and purified on Omix C18 tips (Agilent, catnr. A57003100), dried and re-dissolved in 20 µl loading solvent (0.1% TFA in water/acetonitrile (98:2, v/v)). Five microliters of the peptide mixture was injected for LC-MS/MS analysis on an Ultimate 3000 RSLC nano LC (Thermo, Bremen, Germany) in-line connected to a Q Exactive mass spectrometer

(Thermo). Trapping was performed at 10 µl/min for 4 min in loading solvent on a 100 µm internal diameter (I.D.) × 20 mm trapping column (5 µm beads, C18 Reprosil-HD, Dr. Maisch, Germany) and the sample was loaded on a reverse-phase column (made in-house, 75 µm I.D. x 220 mm, 1.9 µm. Peptides were eluted by a linear increase from 2 to 55% solvent B (0.08% formic acid in water/acetonitrile (2:8, v/v)) over 120 minutes at a constant flow rate of 300 nl/min. The mass spectrometer was operated in data-dependent mode, automatically switching between MS and MS/MS acquisition. Full-scan MS spectra (400-2000 m/z) were acquired at a resolution of 70,000 in the orbitrap analyzer after accumulation to a target value of 3,000,000. The five most intense ions above a threshold value of 17,500 were isolated (window of 2.0 Th) for fragmentation at a normalized collision energy of 25% after filling the trap at a target value of 50,000 for maximum 80 ms. MS/MS spectra (200-2000 m/z) were acquired at a resolution of 17,500 in the orbitrap analyzer. Raw LC-MS/MS data files were searched against the human proteins in the Uniprot/Swiss-Prot database (database version of September 2017 containing 20,237 human sequences, downloaded from www.uniprot.org). The mass tolerance for precursor and fragment ions were set to 4.5 and 20 ppm, respectively, during the main search. Enzyme specificity was set as C-terminal to arginine and lysine, also allowing cleavage at proline bonds with a maximum of two missed cleavages. Variable modifications were set to oxidation of methionine residues, acetylation of protein N-termini, phosphorylation and thiophosphorylation of serine, threonine and tyrosine residues. The minimum score for modified peptides was set to 40. The S-lens RF level was set at 50 and we excluded precursor ions with single, unassigned and charge states above five from fragmentation selection.

Peptide arrays, Peptide SPOT assay of ATG16L1 phosphorylation sites screening

Automatic peptide SPOT synthesis was carried out as described previously(Hundsrucker et al., 2006, 2010; Maass et al., 2015; Stefan et al., 2007). Fmoc-protected amino acids (Merck Millipore) and amino-modified acid-stable cellulose membranes with PEG-spacers (Intavis) were used for peptide spots synthesis on an Intavis ResPep-SL device.

For phosphorylation of the peptides by PKA(Maass et al., 2015), the membranes were activated in ethanol, blocked in blocking buffer (5 % milk in TBS-T: Tris-HCl, 10 mM; NaCl, 150 mM; Tween 20, 0.05 %; pH 7.4) for 3 h at room temperature, and washed twice with incubation buffer (Tris-HCl, 50 mM pH 7.4; $MgCl_2$, 5 mM; ATP, 100 µM). His-tagged recombinant catalytic subunits (vector pET46) were purified from E. coli (strain Rosetta D3) as described(Maass et al., 2015; Schäfer et al., 2013). The membranes were incubated with the recombinant protein (1 nM) or with the cAMP-dependent protein Kinase, catalytic subunit (Promega V5161) (1nM) in incubation buffer (1 h, 30°C), washed three times with TBS-T, and phosphorylated serines were detected with PKA phosphosubstrate antibody directed against the consensus site RRX p(S/T) (Cell Signaling Technology, 100G7E, rabbit mAB #9624) in blocking buffer overnight at 4°C(Christian et al., 2011). The membranes were washed three times with TBS-T, and a secondary horseradish peroxidase (HRP)-coupled donkey anti-rabbit antibody (#711-036-153; Jackson Immuno Research) was added (3 h, RT). After three washs with TBS-T, an ECL system (Immobilon™ Western substrate, Merck Millipore) and an Odyssey FC device (Li-Cor ®) was used for visualizing phosphorylated serines.

Animal procedures

All animal experimental procedures were approved by the Institutional Animal Care and Research Advisory Committee of the University of Leuven and performed according to the European guidelines. Following mouse strains were used: Prkar1a^{tm2Gsm} (Willis, Niswender, Su, Amieux, & McKnight, 2011), Tg(Cdh5-cre/ERT2)^{1Rha} (Wang et al., 2010) and ATG5$^{flox/flox}$ (Hara et al., 2006). All animals used in the experiments were of mixed N/FVB x C57/Bl6 background. Comparisons have been done between littermates only. For chloroquine rescue retinal angiogenesis experiment, pups were intraperitoneally injected with 50 µl of 1mg/ml tamoxifen from postnatal day one (P1) to P3, and 100ul µl of 1.25mg/ml chloroquine or PBS from P1 to P5. Mice were euthanized at P6, and dissection and staining of the retinas were performed as described below. For endothelial cells isolation, pups were intraperitoneally injected with 75 µl of 1mg/ml tamoxifen daily from P7 until P10 and the mice were euthanized at 8 weeks and endothelial cells were isolated as described below.

Retinal angiogenesis assay

To analyse retinal angiogenesis , the procedures of isolation and staining of the retinas were performed as published(Pitulescu, Schmidt, Benedito, & Adams, 2010). Briefly, retinas were dissected in PBS and blocked/permeabilized in retina blocking buffer (1% BSA and 0.3% Triton X-100 in PBS) for 1-2 hours at room temperature. Alexa Fluor^{TM} 488 conjugated Isolectin GS-IB4(Invitrogen) diluted in Pblec solution (1mM $MgCl_2$, 1mM $CaCl_2$, 0.1mM $MnCl_2$ and 1% Triton X-100 in PBS) was added to visualize whole-retina vasculature by incubating overnight at 4°C, followed by staining for ESM1 (primary goat anti-ESM1 antibody; R&D Systems). After mounting, images of retinas were taken using a Leica SPE confocal microscope equipped with a HC PL APO 20X/0.75 IMM CORR CS2 objective or Leica SP8 confocal microscope equipped with a HCX IRAPO L 25X/0.95 W objective. Images were taken at room temperature using Leica LAS X software and processed with image J software.

Endothelial cell isolation from liver or lung

Livers or lung lobes were collected in dry 10cm dishes and minced finely with blades for one minute, and then incubated in 25ml of pre-warmed Dulbecco modified Eagle medium (4.5 g/L glucose with L-glutamine) containing 2 mg/mL collagenase (Invitrogen) in 50 ml tubes, gently shaking for 45 minutes at 37°C. Suspensions were passed through a 70µm cell strainer (VWR) and cells were spun down at 400g for 8 minutes at 4°C. Pellets were resuspended in 10 ml Dulbecco modified Eagle medium containing 10% FBS, 50U/ml penicillin and 50µg/ml streptomycin, passed through 40µm Nylon cell strainer (BD Falcon, Cat. No. 352340) and centrifuged at 400g for 8 minutes at 4°C. Cells were resuspended in cold DPBS (1ml/lung and 2ml/liver), added to sheep anti-Rat IgG-coupled Dynabeads (Invitrogen) pre-incubated with purified Rat Anti-Mouse CD31 (BD Pharmingen) and incubated at 4°C. for 20 min The beads were separated using a magnetic particle concentrator (Dynal MPC-S; Invitrogen)and washed with cold DPBS with 0.1% BSA. This washing step was repeated 5 times after which cells were lysed in RIPA buffer for Western Blotting.

Statistical analysis

Statistical analyses were performed using GraphPad Prism 7. The one-way ANOVA was used to compare more than two experimental groups.

Acknowledgments

We are grateful to Evy Timmerman and Francis Impens for their help to identify the phosphorylation sites of ATG16L1 in MS analysis at the VIB proteomics core facility. This work was supported by grants from the Fonds voor Wetenschappelijk Onderzoek (FWO) [G.0742.15N to H.G]; the Vlaams Instituut voor Biotechnologie (VIB) Tech watch grant [Q3 2015 to P.I.N]; the Elsa-Kroener-Stiftung [2014_A26 to H.G and P.I.N]; the European Research Consortil [ERC Consolidator grant REshape 311719 to H.G]; This work was supported by grants from the German Centre for Cardiovascular Research (DZHK) partner site Berlin (81XZ100146), the Deutsche Forschungsgemeinschaft (DFG KL1415/7-1 and 394046635 – SFB 1365) and the Bundesministerium für Bildung und Forschung (BMBF; 16GW0179K) to EK.

References

Alaimo, P. J., Shogren-Knaak, M. a, & Shokat, K. M. (2001). Chemical genetic approaches for the elucidation of signaling pathways. *Current Opinion in Chemical Biology*, *5*(4), 360–367. https://doi.org/10.1016/S1367-5931(00)00215-5

Allen, J. J., Lazerwith, S. E., & Shokat, K. M. (2005). Bio-orthogonal affinity purification of direct kinase substrates. *Journal of the American Chemical Society*, *127*(15), 5288–5289. https://doi.org/10.1021/ja050727t

Allen, J. J., Li, M., Brinkworth, C. S., Paulson, J. L., Wang, D., Hübner, A., … Shokat, K. M. (2007). A semisynthetic epitope for kinase substrates. *Nature Methods*, *4*(6), 511–516. https://doi.org/10.1038/nmeth1048

Anton, K. A., Sinclair, J., Ohoka, A., Kajita, M., Ishikawa, S., Benz, P. M., … Fujita, Y. (2014). PKA-regulated VASP phosphorylation promotes extrusion of transformed cells from the epithelium. *Journal of Cell Science*, *127*(16), 3425–3433. https://doi.org/10.1242/jcs.149674

Banko, M. R., Allen, J. J., Schaffer, B. E., Wilker, E. W., Tsou, P. P., White, J. L., … Brunet, A. (2011). Chemical Genetic Screen for AMPKα2 Substrates Uncovers a Network of Proteins Involved in Mitosis. *Molecular Cell*, *44*(6), 878–892. https://doi.org/10.1016/j.molcel.2011.11.005

Bullen, J. W., Tchernyshyov, I., Holewinski, R. J., Devine, L., Wu, F., Venkatraman, V., … Semenza, G. L. (2016). Protein kinase A – dependent phosphorylation stimulates the transcriptional activity of hypoxia-inducible factor 1. *Science Signaling*, *9*(430), 1–13. https://doi.org/10.1126/scisignal.aaf0583

Butt, E., Abel, K., Krieger, M., Palm, D., Hoppe, V., Hoppe, J., & Walter, U. (1994). cAMP- and cGMP-dependent protein kinase phosphorylation sites of the focal adhesion vasodilator-stimulated phosphoprotein (VASP) in vitro and in intact

human platelets. *Journal of Biological Chemistry*, *269*(20), 14509–14517.

C. Manning, D.B. Whyte, R. Martinez, T. hunter, S. S. (2002). The Protein Kinase Complement of the Human Genome: EBSCOhost. *Sciencemag.Org*, *298*(5600), 1912–1934. https://doi.org/10.1126/science.1075762

Cadwell, K., Liu, J. Y., Brown, S. L., Miyoshi, H., Loh, J., Lennerz, J. K., … Virgin IV, H. W. (2008). A key role for autophagy and the autophagy gene Atg16l1 in mouse and human intestinal Paneth cells. *Nature*, *456*(7219), 259–263. https://doi.org/10.1038/nature07416

Cao, R., Farnebo, J., Kurimoto, M., & Cao, Y. (1999). Interleukin-18 acts as an angiogenesis and tumor suppressor. *Faseb J*, *13*(15), 2195–2202. Retrieved from http://www.ncbi.nlm.nih.gov/pubmed/10593867

Carmi, Y., Dotan, S., Rider, P., Kaplanov, I., White, M. R., Baron, R., … Voronov, E. (2013). The Role of IL-1 in the Early Tumor Cell-Induced Angiogenic Response. *The Journal of Immunology*, *190*(7), 3500–3509. https://doi.org/10.4049/jimmunol.1202769

Cheng, N., Brantley, D. M., & Chen, J. (2002). The ephrins and Eph receptors in angiogenesis. *Cytokine and Growth Factor Reviews*, *13*(1), 75–85. https://doi.org/10.1016/S1359-6101(01)00031-4

Cherra, S. J., Kulich, S. M., Uechi, G., Balasubramani, M., Mountzouris, J., Day, B. W., & Chu, C. T. (2010). Regulation of the autophagy protein LC3 by phosphorylation. *Journal of Cell Biology*, *190*(4), 533–539. https://doi.org/10.1083/jcb.201002108

Christian, F., Szaszák, M., Friedl, S., Drewianka, S., Lorenz, D., Goncalves, A., … Klussmann, E. (2011). Small molecule AKAP-Protein Kinase A (PKA) interaction disruptors that activate PKA interfere with compartmentalized cAMP signaling in cardiac myocytes. *Journal of Biological Chemistry*. https://doi.org/10.1074/jbc.M110.160614

Cox, J., Hein, M. Y., Luber, C. A., Paron, I., Nagaraj, N., & Mann, M. (2014). Accurate Proteome-wide Label-free Quantification by Delayed Normalization and Maximal Peptide Ratio Extraction, Termed MaxLFQ. *Molecular & Cellular Proteomics*. https://doi.org/10.1074/mcp.M113.031591

Cox, J., & Mann, M. (2008). MaxQuant enables high peptide identification rates, individualized p.p.b.-range mass accuracies and proteome-wide protein quantification. *Nature Biotechnology*. https://doi.org/10.1038/nbt.1511

Cox, J., Neuhauser, N., Michalski, A., Scheltema, R. A., Olsen, J. V., & Mann, M. (2011). Andromeda: A peptide search engine integrated into the MaxQuant environment. *Journal of Proteome Research*. https://doi.org/10.1021/pr101065j

Diamanti, M. A., Gupta, J., Bennecke, M., De Oliveira, T., Ramakrishnan, M., Braczynski, A. K., … Greten, F. R. (2017). IKKα controls ATG16L1 degradation to prevent ER stress during inflammation. *The Journal of Experimental Medicine*, *214*(2), 423–437. https://doi.org/10.1084/jem.20161867

Du, J., Teng, R.-J., Guan, T., Eis, A., Kaul, S., Konduri, G. G., & Shi, Y. (2012). Role of autophagy in angiogenesis in aortic endothelial cells. *AJP: Cell Physiology*, *302*(2), C383–C391. https://doi.org/10.1152/ajpcell.00164.2011

Ferrara, N., Gerber, H. P., & LeCouter, J. (2003). The biology of VEGF and its receptors. *Nature Medicine*, *9*(6), 669–676. https://doi.org/10.1038/nm0603-669

Geng, H., Wittwer, T., Dittrich-Breiholz, O., Kracht, M., & Schmitz, M. L. (2009). Phosphorylation of NF-κB p65 at Ser468 controls its COMMD1-dependent ubiquitination and target gene-specific proteasomal elimination. *EMBO Reports*, *10*(4), 381–386. https://doi.org/10.1038/embor.2009.10

Gerhardt, H., Golding, M., Fruttiger, M., Ruhrberg, C., Lundkvist, A., Abramsson, A., … Betsholtz, C. (2003). VEGF guides angiogenic sprouting utilizing endothelial tip cell filopodia. *Journal of Cell Biology*, *161*(6), 1163–1177. https://doi.org/10.1083/jcb.200302047

Geudens, I., & Gerhardt, H. (2011). Coordinating cell behaviour during blood vessel formation. *Development*, *138*(21), 4569–4583. https://doi.org/10.1242/dev.062323

Hara, T., Nakamura, K., Matsui, M., Yamamoto, A., Nakahara, Y., Suzuki-Migishima, R., … Mizushima, N. (2006). Suppression of basal autophagy in neural cells causes neurodegenerative disease in mice. *Nature*, *441*(7095), 885–889. https://doi.org/10.1038/nature04724

Hellström, M., Phng, L. K., Hofmann, J. J., Wallgard, E., Coultas, L., Lindblom, P., … Betsholtz, C. (2007). Dll4 signalling through Notch1 regulates formation of tip cells during angiogenesis. *Nature*, *445*(7129), 776–780. https://doi.org/10.1038/nature05571

Hundsrucker, C., Krause, G., Beyermann, M., Prinz, A., Zimmermann, B., Diekmann, O., … Klussmann, E. (2006). High-affinity AKAP7δ–protein kinase A interaction yields novel protein kinase A-anchoring disruptor peptides. *Biochemical Journal*. https://doi.org/10.1042/BJ20051970

Hundsrucker, C., Skroblin, P., Christian, F., Zenn, H. M., Popara, V., Joshi, M., … Klussman, E. (2010). Glycogen synthase kinase 3β interaction protein functions as an a-kinase anchoring protein. *Journal of Biological Chemistry*. https://doi.org/10.1074/jbc.M109.047944

Hunter, T. (1995). Protein kinases and phosphatases: The Yin and Yang of protein phosphorylation and signaling. *Cell*, *80*(2), 225–236. https://doi.org/10.1016/0092-8674(95)90405-0

Hwang, C. Y., Lee, C., & Kwon, K.-S. (2009). Extracellular Signal-Regulated Kinase 2-Dependent Phosphorylation Induces Cytoplasmic Localization and Degradation of p21Cip1. *Molecular and Cellular Biology*, *29*(12), 3379–3389. https://doi.org/10.1128/MCB.01758-08

Kennelly, P. J., & Krebs, E. G. (1991). Consensus sequences as substrate specificity determinants for protein kinases and protein phosphatases. *Journal of Biological*

Chemistry, *266*(24), 15555–15558. https://doi.org/10.1378/chest.118.4.1083

Kim, J., Lim, D., Koh, G. Y., Kim, J., Kim, Y. H., Kim, J., … Kim, K. H. (2017). YAP / TAZ regulates sprouting angiogenesis and vascular barrier maturation Find the latest version : YAP / TAZ regulates sprouting angiogenesis and vascular barrier maturation, *127*(9), 3441–3461.

Kuma, A., Mizushima, N., Ishihara, N., & Ohsumi, Y. (2002). Formation of the ???350-kDa Apg12-Apg5??Apg16 multimeric complex, mediated by Apg16 oligomerization, is essential for autophagy in yeast. *Journal of Biological Chemistry*, *277*(21), 18619–18625. https://doi.org/10.1074/jbc.M111889200

Lee, M. Y., Luciano, A. K., Ackah, E., Rodriguez-Vita, J., Bancroft, T. A., Eichmann, A., … Sessa, W. C. (2014). Endothelial Akt1 mediates angiogenesis by phosphorylating multiple angiogenic substrates. *Proceedings of the National Academy of Sciences*, *111*(35), 12865–12870. https://doi.org/10.1073/pnas.1408472111

Leslie, J. D., Ariza-McNaughton, L., Bermange, A. L., McAdow, R., Johnson, S. L., & Lewis, J. (2007). Endothelial signalling by the Notch ligand Delta-like 4 restricts angiogenesis. *Development*, *134*(5), 839–844. https://doi.org/10.1242/dev.003244

Levine, B., & Kroemer, G. (2008). Autophagy in the Pathogenesis of Disease. *Cell*, *132*(1), 27–42. https://doi.org/10.1016/j.cell.2007.12.018

Liang, P., Jiang, B., Li, Y., Liu, Z., Zhang, P., Zhang, M., … Xiao, X. (2018). Autophagy promotes angiogenesis via AMPK/Akt/mTOR signaling during the recovery of heat-denatured endothelial cells. *Cell Death & Disease*, *9*(12), 1152. https://doi.org/10.1038/s41419-018-1194-5

Liu, J., Wada, Y., Katsura, M., Tozawa, H., Erwin, N., Kapron, C. M., … Liu, J. (2018). Rho-Associated Coiled-Coil Kinase (ROCK) in Molecular Regulation of Angiogenesis. *Theranostics*, *8*(21), 6053–6069. https://doi.org/10.7150/thno.30305

Lobov, I. B., Renard, R. A., Papadopoulos, N., Gale, N. W., Thurston, G., Yancopoulos, G. D., & Wiegand, S. J. (2007). Delta-like ligand 4 (Dll4) is induced by VEGF as a negative regulator of angiogenic sprouting. *Proceedings of the National Academy of Sciences*, *104*(9), 3219–3224. https://doi.org/10.1073/pnas.0611206104

Lu, Q., Yao, Y., Hu, Z., Hu, C., Song, Q., Ye, J., … Wang, Q. K. (2016). Angiogenic Factor AGGF1 Activates Autophagy with an Essential Role in Therapeutic Angiogenesis for Heart Disease. *PLoS Biology*. https://doi.org/10.1371/journal.pbio.1002529

Maass, P. G., Aydin, A., Luft, F. C., Schächterle, C., Weise, A., Stricker, S., … Bähring, S. (2015). PDE3A mutations cause autosomal dominant hypertension with brachydactyly. *Nature Genetics*. https://doi.org/10.1038/ng.3302

Manni, S., Mauban, J. H., Ward, C. W., & Bond, M. (2008). Phosphorylation of the

cAMP-dependent protein kinase (PKA) regulatory subunit modulates PKA-AKAP interaction, substrate phosphorylation, and calcium signaling in cardiac cells. *Journal of Biological Chemistry*, *283*(35), 24145–24154. https://doi.org/10.1074/jbc.M802278200

Matsushita, M., Suzuki, N. N., Obara, K., Fujioka, Y., Ohsumi, Y., & Inagaki, F. (2007). Structure of Atg5??Atg16, a complex essential for autophagy. *Journal of Biological Chemistry*, *282*(9), 6763–6772. https://doi.org/10.1074/jbc.M609876200

Mizushima, N. (2003). Mouse Apg16L, a novel WD-repeat protein, targets to the autophagic isolation membrane with the Apg12-Apg5 conjugate. *Journal of Cell Science*, *116*(9), 1679–1688. https://doi.org/10.1242/jcs.00381

Mizushima, N. (2010). The role of the Atg1/ULK1 complex in autophagy regulation. *Current Opinion in Cell Biology*, *22*(2), 132–139. https://doi.org/10.1016/j.ceb.2009.12.004

Mizushima, N., Noda, T., & Ohsumi, Y. (1999). Apg16p is required for the function of the Apg12p-Apg5p conjugate in the yeast autophagy pathway. *EMBO Journal*, *18*(14), 3888–3896. https://doi.org/10.1093/emboj/18.14.3888

Montalvo, J., Spencer, C., Hackathorn, A., Masterjohn, K., Perkins, A., Doty, C., … Bryan, B. A. (2013). Rock1 & 2 Perform Overlapping and Unique Roles in Angiogenesis and Angiosarcoma Tumor Progression. *Curr Mol Med*, *1*, 205–219.

Murthy, A., Li, Y., Peng, I., Reichelt, M., Katakam, A. K., Noubade, R., … Van Lookeren Campagne, M. (2014). A Crohn's disease variant in Atg16l1 enhances its degradation by caspase 3. *Nature*, *506*(7489), 456–462. https://doi.org/10.1038/nature13044

Nedvetsky, P. I., Zhao, X., Mathivet, T., Aspalter, I. M., Stanchi, F., Metzger, R. J., … Gerhardt, H. (2016). cAMP-dependent protein kinase A (PKA) regulates angiogenesis by modulating tip cell behavior in a Notch-independent manner. *Development*, *143*(19), 3582–3590. https://doi.org/10.1242/dev.134767

Neto, F., Klaus-Bergmann, A., Ong, Y. T., Alt, S., Vion, A. C., Szymborska, A., … Gerhardt, H. (2018). YAP and TAZ regulate adherens junction dynamics and endothelial cell distribution during vascular development. *ELife*, *7*, 1–30. https://doi.org/10.7554/eLife.31037

Niswender, C. M., Ishihara, R. W., Judge, L. M., Zhang, C., Shokat, K. M., & McKnight, G. S. (2002). Protein engineering of protein kinase A catalytic subunits results in the acquisition of novel inhibitor sensitivity. *The Journal of Biological Chemistry*, *277*(32), 28916–28922. https://doi.org/10.1074/jbc.M203327200

Pitulescu, M. E., Schmidt, I., Benedito, R., & Adams, R. H. (2010). Inducible gene targeting in the neonatal vasculature and analysis of retinal angiogenesis in mice. *Nature Protocols*, *5*(9), 1518–1534. https://doi.org/10.1038/nprot.2010.113

Pola, R., Ling, L. E., Silver, M., Corbley, M. J., Kearney, M., Blake Pepinsky, R., …

Isner, J. M. (2001). The morphogen Sonic hedgehog is an indirect angiogenic agent upregulating two families of angiogenic growth factors. *Nature Medicine*, *7*(6), 706–711. https://doi.org/10.1038/89083

Potente, M., Gerhardt, H., & Carmeliet, P. (2011). Basic and therapeutic aspects of angiogenesis. *Cell*, *146*(6), 873–887. https://doi.org/10.1016/j.cell.2011.08.039

Profirovic, J., Gorovoy, M., Niu, J., Pavlovic, S., & Voyno-Yasenetskaya, T. (2005). A novel mechanism of G protein-dependent phosphorylation of vasodilator-stimulated phosphoprotein. *Journal of Biological Chemistry*, *280*(38), 32866–32876. https://doi.org/10.1074/jbc.M501361200

Saitoh, T., Fujita, N., Jang, M. H., Uematsu, S., Yang, B. G., Satoh, T., … Akira, S. (2008). Loss of the autophagy protein Atg16L1 enhances endotoxin-induced IL-1β production. *Nature*, *456*(7219), 264–268. https://doi.org/10.1038/nature07383

Satyanarayana, A., Gudmundsson, K. O., Chen, X., Coppola, V., Tessarollo, L., Keller, J. R., & Hou, S. X. (2010). RapGEF2 is essential for embryonic hematopoiesis but dispensable for adult hematopoiesis. *Blood*, *116*(16), 2921–2931. https://doi.org/10.1182/blood-2010-01-262964

Schäfer, G., Milič, J., Eldahshan, A., Götz, F., Zühlke, K., Schillinger, C., … Klussmann, E. (2013). Highly functionalized terpyridines as competitive inhibitors of AKAP-PKA interactions. *Angewandte Chemie - International Edition*. https://doi.org/10.1002/anie.201304686

Seto, S.-W., Chang, D., Jenkins, A., Bensoussan, A., & Kiat, H. (2016). Angiogenesis in Ischemic Stroke and Angiogenic Effects of Chinese Herbal Medicine. *Journal of Clinical Medicine*, *5*(6), 56. https://doi.org/10.3390/jcm5060056

Shevchenko, A., Tomas, H., Havliš, J., Olsen, J. V., & Mann, M. (2007). In-gel digestion for mass spectrometric characterization of proteins and proteomes. *Nature Protocols*. https://doi.org/10.1038/nprot.2006.468

Shimizu, T., Fukumoto, Y., Tanaka, S. I., Satoh, K., Ikeda, S., & Shimokawa, H. (2013). Crucial role of ROCK2 in vascular smooth muscle cells for hypoxia-induced pulmonary hypertension in mice. *Arteriosclerosis, Thrombosis, and Vascular Biology*, *33*(12), 2780–2791. https://doi.org/10.1161/ATVBAHA.113.301357

Song, H., Pu, J., Wang, L., Wu, L., Xiao, J., Liu, Q., … Zhang, Z. (2015). ATG16L1 phosphorylation is oppositely regulated by CSNK2/casein kinase 2 and PPP1/protein phosphatase 1 which determines the fate of cardiomyocytes during hypoxia/reoxygenation. *Autophagy*, *11*(8), 1308–1325. https://doi.org/10.1080/15548627.2015.1060386

Sorbara, M. T., Ellison, L. K., Ramjeet, M., Travassos, L. H., Jones, N. L., Girardin, S. E., & Philpott, D. J. (2013). The protein ATG16L1 suppresses inflammatory cytokines induced by the intracellular sensors Nod1 and Nod2 in an autophagy-

independent manner. *Immunity*, *39*(5), 858–873. https://doi.org/10.1016/j.immuni.2013.10.013

Stefan, E., Wiesner, B., Baillie, G. S., Mollajew, R., Henn, V., Lorenz, D., … Klussmann, E. (2007). Compartmentalization of cAMP-Dependent Signaling by Phosphodiesterase-4D Is Involved in the Regulation of Vasopressin-Mediated Water Reabsorption in Renal Principal Cells. *Journal of the American Society of Nephrology*. https://doi.org/10.1681/ASN.2006020132

Suchting, S., Freitas, C., le Noble, F., Benedito, R., Breant, C., Duarte, A., & Eichmann, A. (2007). The Notch ligand Delta-like 4 negatively regulates endothelial tip cell formation and vessel branching. *Proceedings of the National Academy of Sciences*, *104*(9), 3225–3230. https://doi.org/10.1073/pnas.0611177104

Ubersax, J. A., & Ferrell, J. E. (2007). Mechanisms of specificity in protein phosphorylation. *Nature Reviews Molecular Cell Biology*, *8*(7), 530–541. https://doi.org/10.1038/nrm2203

Vion, A. C., Alt, S., Klaus-Bergmann, A., Szymborska, A., Zheng, T., Perovic, T., … Gerhardt, H. (2018). Primary cilia sensitize endothelial cells to BMP and prevent excessive vascular regression. *Journal of Cell Biology*, *217*(5), 1651–1665. https://doi.org/10.1083/jcb.201706151

Vitorino, P., Yeung, S., Crow, A., Bakke, J., Smyczek, T., West, K., … Ye, W. (2015). MAP4K4 regulates integrin-FERM binding to control endothelial cell motility. *Nature*, *519*(7544), 425–430. https://doi.org/10.1038/nature14323

Voronov, E., Shouval, D. S., Krelin, Y., Cagnano, E., Benharroch, D., Iwakura, Y., … Apte, R. N. (2003). IL-1 is required for tumor invasiveness and angiogenesis. *Proceedings of the National Academy of Sciences*, *100*(5), 2645–2650. https://doi.org/10.1073/pnas.0437939100

Wang, Y., Nakayama, M., Pitulescu, M. E., Schmidt, T. S., Bochenek, M. L., Sakakibara, A., … Adams, R. H. (2010). Ephrin-B2 controls VEGF-induced angiogenesis and lymphangiogenesis. *Nature*, *465*(7297), 483–486. https://doi.org/10.1038/nature09002

Willis, B. S., Niswender, C. M., Su, T., Amieux, P. S., & McKnight, G. S. (2011). Cell-type specific expression of a dominant negative PKA mutation in mice. *PLoS ONE*, *6*(4). https://doi.org/10.1371/journal.pone.0018772

Xing, Y., Tian, Y., Kurosawa, T., Matsui, S., Touma, M., Wu, Q., & Sugimoto, K. (2016). Inhibition of blood vessel formation in tumors by IL-18-polarized M1 macrophages. *Genes to Cells*, *21*(3), 287–295. https://doi.org/10.1111/gtc.12329

Yang, S., Chen, X. Q., Lu, H. S., Li, Z. Y., & Lin, T. Y. (2010). Interleukin-18 suppresses angiogenesis and lymphangiogenesis in implanted Lewis lung cancer. *Chinese Journal of Cancer Research*, *22*(4), 303–309. https://doi.org/10.1007/s11670-010-0303-5

Figure 1

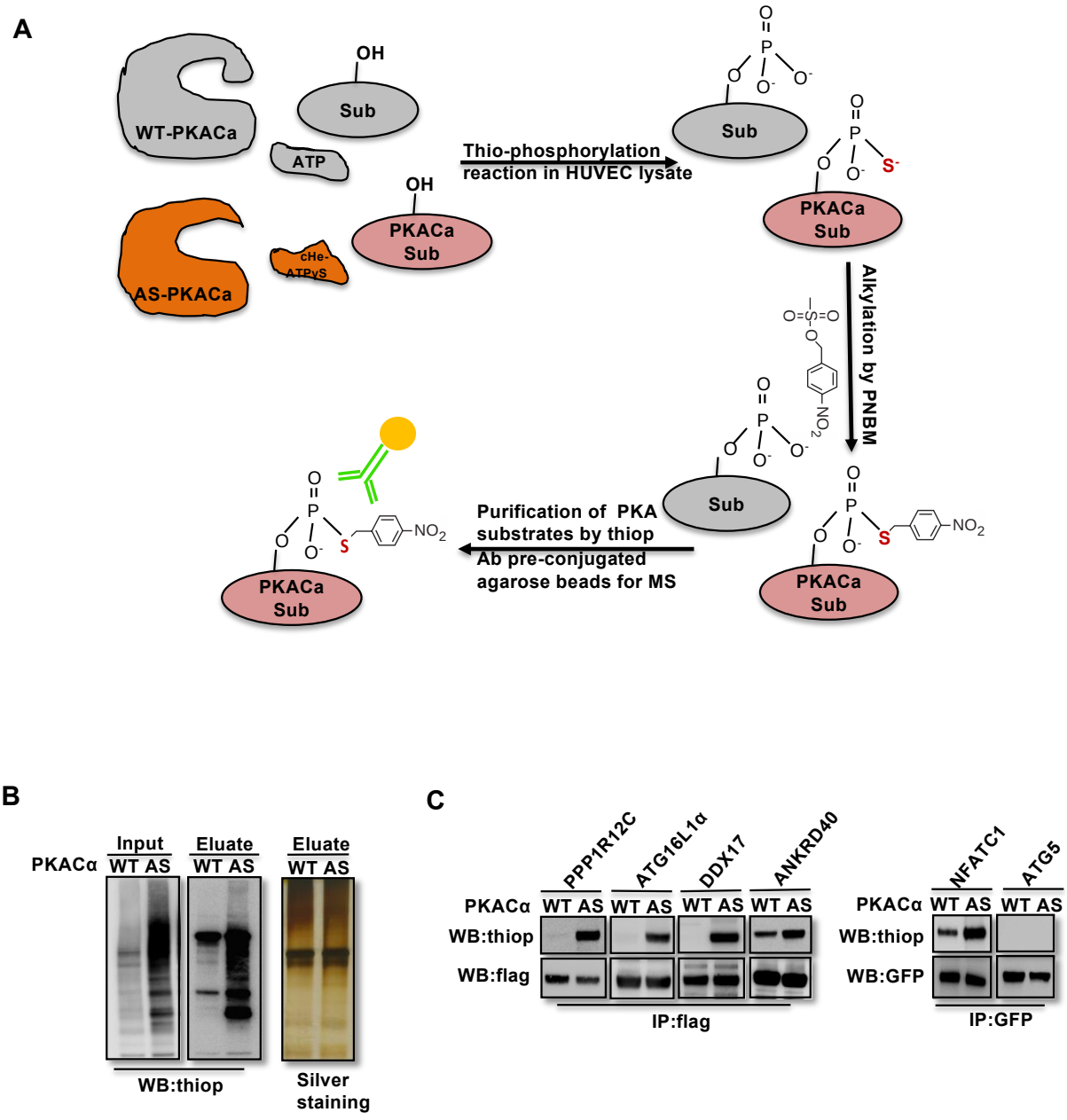

Figure 1. Identification of direct substrates of PKACα. **(A)**Strategy for labeling, immunoprecipitation and identifying of PKACα substrates in HUVEC lysates. **(B)**Thio-phosphorylation of PKA substrates in HUVEC lysates expressing WT-PKACα or AS-PKACα for mass spectrometry analysis. Left panel (input) shows western blot analysis of lysates after alkylation before immunoprecipitation, middle panel (Elute) shows western blot analysis of the eluted proteins from the immunoprecipitation beads, right panel (Elute) shows the silver staining of the same samples as middle panel. **(C)**Validation of the six PKACα substrates identified in the chemical genetic approach screen by overexpressing of potential substrates and WT-PKACα (or AS-PKACα) in 293Tcells, and labeling the substrate in 293T cell lysates. Western blots are representative of two independent experiments.

Table 1. List of PKACa substrates

Uniprot	Protein.names	Gene.names	Peptides	Log ratio AS/WT	
				experiment1	experiment2
Q6AI12	Ankyrin repeat domain-containing protein 40	ANKRD40	9	10	10
Q6P6C2	RNA demethylase ALKBH5	ALKBH5	6	10	10
Q9NRY4	Rho GTPase-activating protein 35	ARHGAP35	9	10	10
E7EVC7	Autophagy-related protein 16-1	ATG16L1	8	10	10
J3KPC8	Serine/threonine-protein kinase SIK3	SIK3;KIAA0999	5	10	10
A1X283	SH3 and PX domain-containing protein 2B	SH3PXD2B	4	10	10
Q8IWZ8	SURP and G-patch domain-containing protein 1	SUGP1	5	10	10
Q9UJX5	Anaphase-promoting complex subunit 4	ANAPC4	5	10	10
O43719	HIV Tat-specific factor 1	HTATSF1	4	10	10
O95644-5	Nuclear factor of activated T-cells, cytoplasmic 1	NFATC1	5	10	10
G8JLI6	Prolyl 3-hydroxylase 3	LEPREL2	3	10	10
F8W781	Zinc finger CCCH domain-containing protein 13	ZC3H13	3	10	10
Q9BZL4	Protein phosphatase 1 regulatory subunit 12C	PPP1R12C	21	6,04440274	7,30701515
O14974	Protein phosphatase 1 regulatory subunit 12A	PPP1R12A	26	5,72796034	7,12654716
Q00537	Cyclin-dependent kinase 17	CDK17	31	6,37867381	6,39216838
Q9Y4G8	Rap guanine nucleotide exchange factor 2	RAPGEF2	21	10	6,17455504
Q9BYB0	SH3 and multiple ankyrin repeat domains protein 3	SHANK3	32	5,26591421	5,6389181
J3KSW8	Myosin phosphatase Rho-interacting protein	MPRIP	18	4,61398477	5,61155414
P31323	cAMP-dependent protein kinase type II-beta regulatory subunit	PRKAR2B	19	7,05077105	5,33509437
P13861	cAMP-dependent protein kinase type II-alpha regulatory subunit	PRKAR2A	24	5,42841998	5,04010629
Q14980-2	Nuclear mitotic apparatus protein 1	NUMA1	61	3,45625969	4,47466712
O15056	Synaptojanin-2	SYNJ2	13	4,64022655	4,46069701
J3KNX9	Unconventional myosin-XVIIIa	MYO18A	10	10	4,43208178
Q86UU1-2	Pleckstrin homology-like domain family B member 1	PHLDB1	19	5,4105243	4,10782285
P28715	DNA repair protein complementing XP-G cells	ERCC5;BIVM-ERCC5	8	3,3571826	4,09305592
P12270	Nucleoprotein TPR	TPR	104	3,3333472	4,04477536
Q15111	Inactive phospholipase C-like protein 1; Phosphoinositide phospholipase C	PLCL1	10	10	3,32188704
Q9HD67	Unconventional myosin-X	MYO10	39	4,13973415	3,21827463
Q14185	Dedicator of cytokinesis protein 1	DOCK1	34	4,50413426	3,18515106
O75116	Rho-associated protein kinase 2	ROCK2	29	3,27701864	3,08277835

Proteins are listed according to the log of fold changes of AS-PKACα to WT PKACα. Two independent experiments have been done to prepare the PKACα substrates samples for mass spectrometric analysis. The full list of proteins identified in both experiments is provided in Table S1.

Figure 2

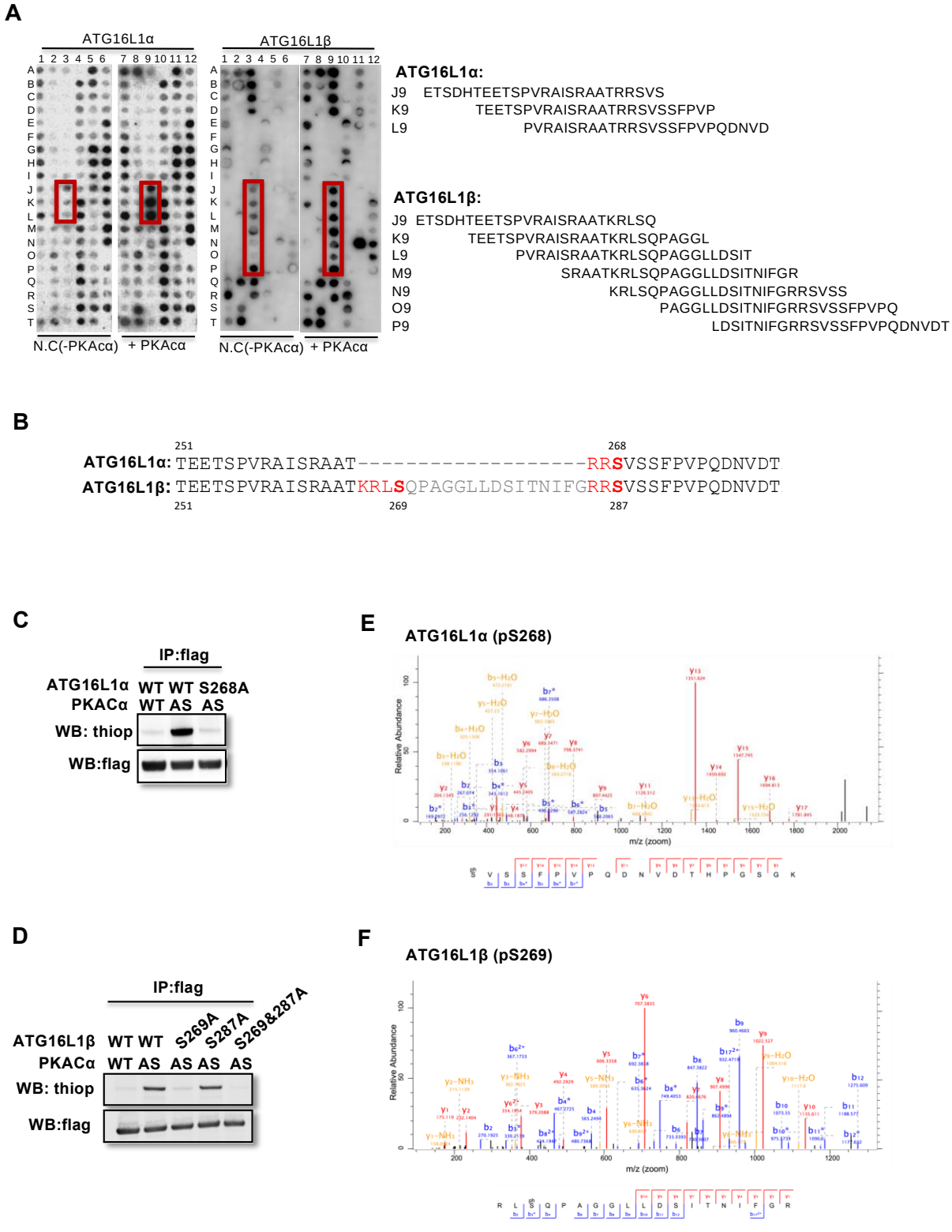

Figure 2.PKACα phosphorylates ATG16L1α at S268 and ATG16L1β at S269. (A) Peptide SPOT assay of ATG16L1 phosphorylation sites screening. **(B)**Amino acid sequence including potential PKACα phosphorylation sites in ATG16L1α and ATG16L1β according to the peptide SPOT assay result of Figure 2A. **(C-D)**Identification of PKACα phosphorylation site in ATG16L1α(C) and ATG16L1β(D). Analysis was performed as in Figure 1C. Western blots are representative of two independent experiments. **(E-F)**Flag tagged ATG16L1α and ATG16L1β were thio-phosphorylated by

AS-PKACα and purified twice using M2 beads and thioP antibody coupled beads, followed by mass spectrometric analysis. LC-MS/MS spectra of the PKA- phosphorylated ATG16L1α tryptic peptide pSVSSFPVPQDNVDTHPGSGK and ATG16L1β tryptic peptide RLpSQPAGGLLDSITNIFGR. The results demonstrate that PKA phosphorylated ATG16L1α at S268 and phosphorylated ATG16L1β at S269.

Figure 3

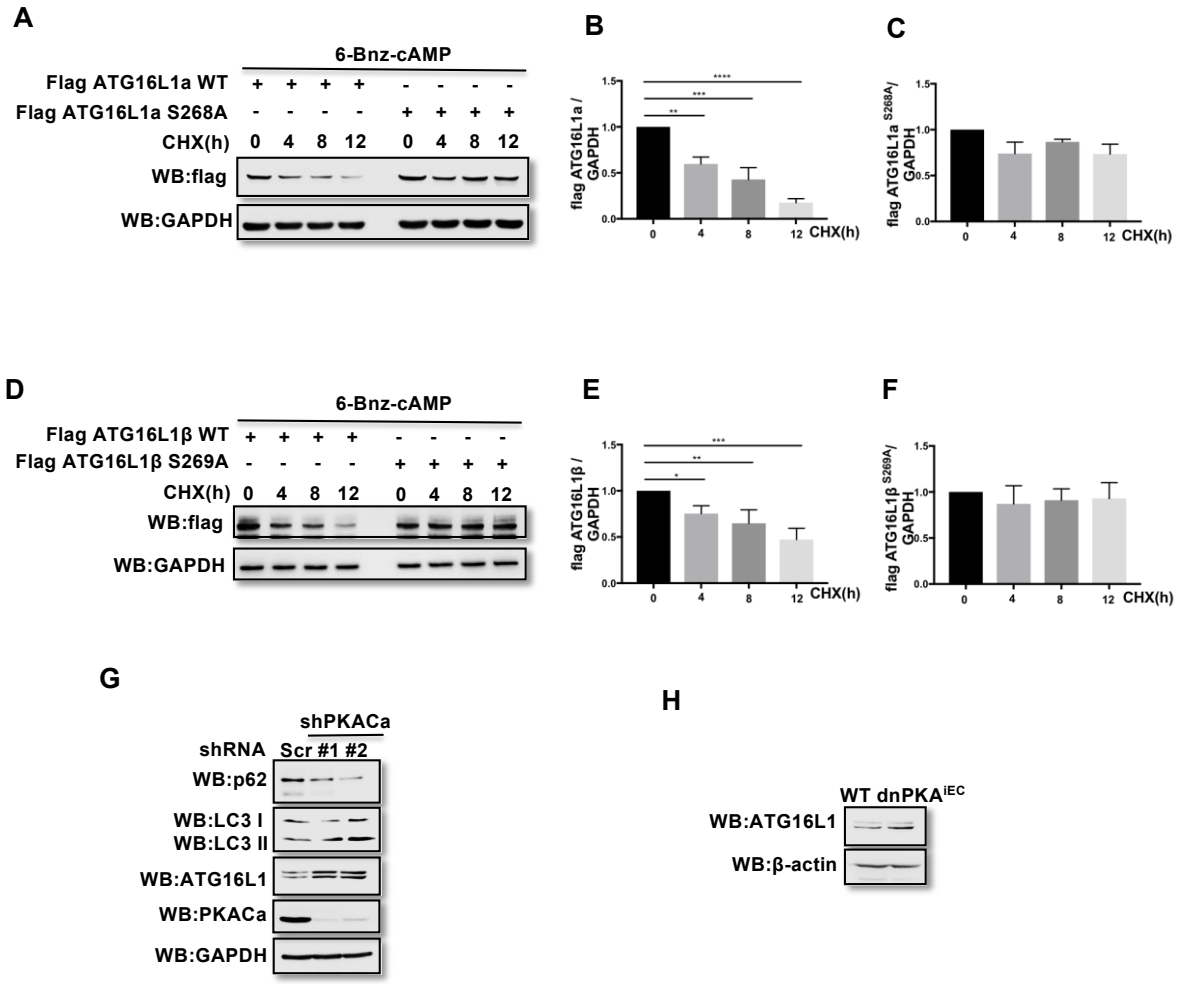

Figure 3. PKACα mediated phosphorylation of ATG16L1 facilitates its degradation whereas PKA deficiency stabilizes ATG16L1. (A-C) HUVECs infected with Flag ATG16L1a (WT or S268A) were treated with 250 mM 6-bnz-cAMP and 20 mg/ml CHX at the time points indicated when they reached confluence(A). Quantifications of Flag ATG16L1a WT(B) and S268A (C) expression. Data present the mean ± SD of 3 independent experiments. **P<0,01; ***P<0,001; ****P<0,0001. **(D-F)** HUVECs infected with Flag ATG16L1β (WT or S269A) were treated with 250 mM 6-bnz-cAMP and 20 mg/ml CHX at the time points indicated when they reached confluence(D). Quantifications of Flag ATG16L1β WT(E) and S269A (F) expression. Data present the mean ± SD of 3 independent experiments. *P<0,05; **P<0,01; ***P<0,001. **(G)** HUVECs infected with shRNA(scramble or shPKACα) virus were lysed in RIPA buffer and proteins were analyzed by western blot using indicated antibodies. Western blots are representative of three independent experiments. **(H)** Endothelial cells isolated from mice(wild type or dnPKA^{iEC}) were lysed in RIPA buffer and ATG16L1 protein was analyzed by western blot.

Figure 4

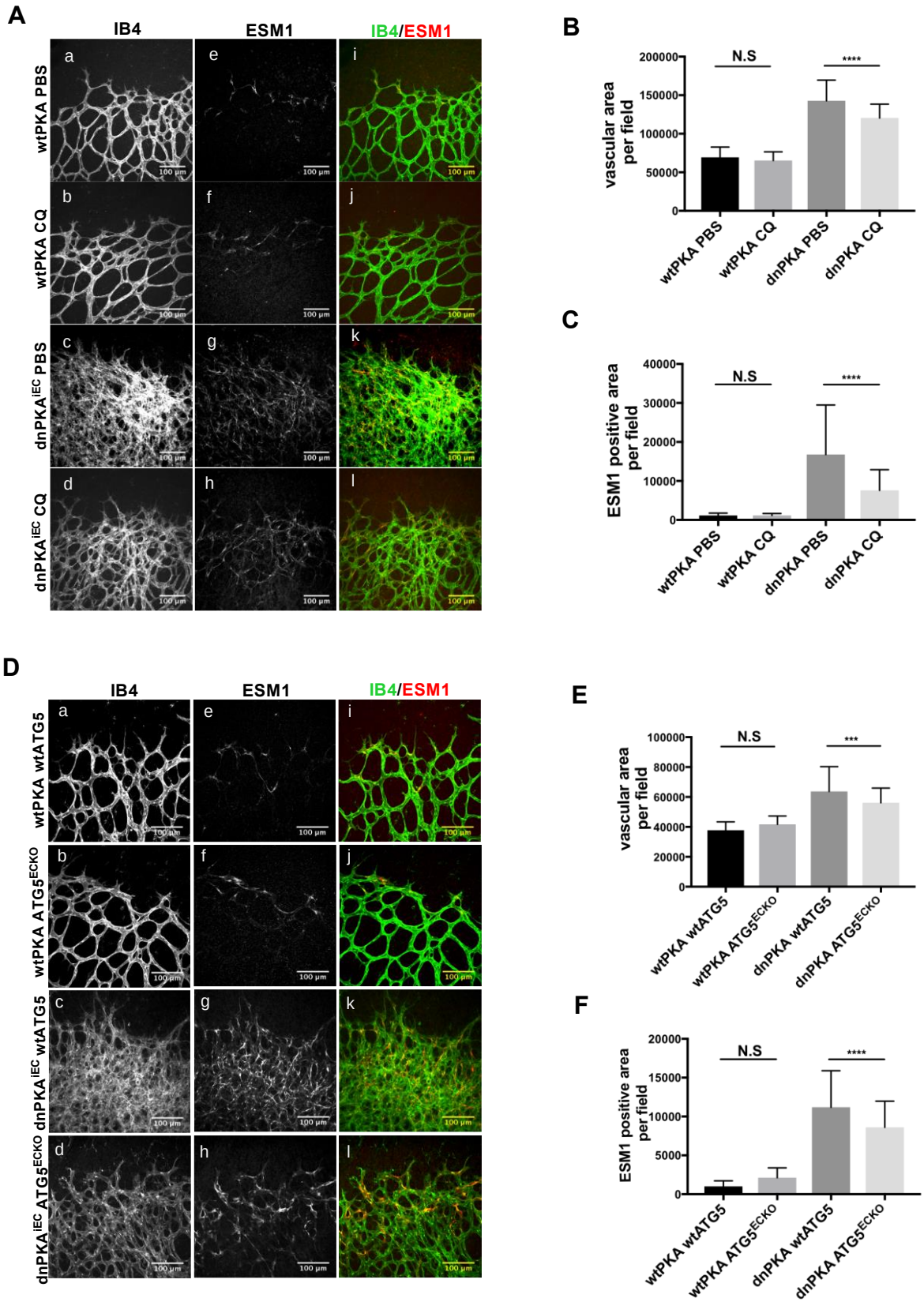

Figure 4. Autophagy inhibition partially rescues retinal vascular hypersprouting caused by PKA deficiency. (A) Mice were injected with tamoxifen from P1 to P3, and retinas were collected at P6. Isolectin B4 and ESM1 staining of P6 retinas isolated from wtPKA and dnPKA^{iEC} mice treated with PBS or CQ. Representative images are shown. **(B-C)** Quantifications of vascular area(B) and ESM1 positive area (C) per field of retinal fronts. 30-35 fields(images) taken from 6-7 retinas were measured for each group, ****P<0,0001. **(D)** Mice were injected with tamoxifen from P1 to P3, then retinas were collected at P6. Isolectin B4 and ESM1 staining of P6 retinas isolated from wtPKA with wtATG5 or ATG5^{ECKO} mice and dnPKA^{iEC} with wtATG5 or ATG5^{ECKO} mice. Representative images are shown. **(E-F)** Quantifications of vascular area(B) and ESM1 positive area (C) per field of retinal fronts. Over 50 fields(images) taken from 8-10 retinas were measured for each group, ***P<0,001;****P<0,0001.

Figure S1

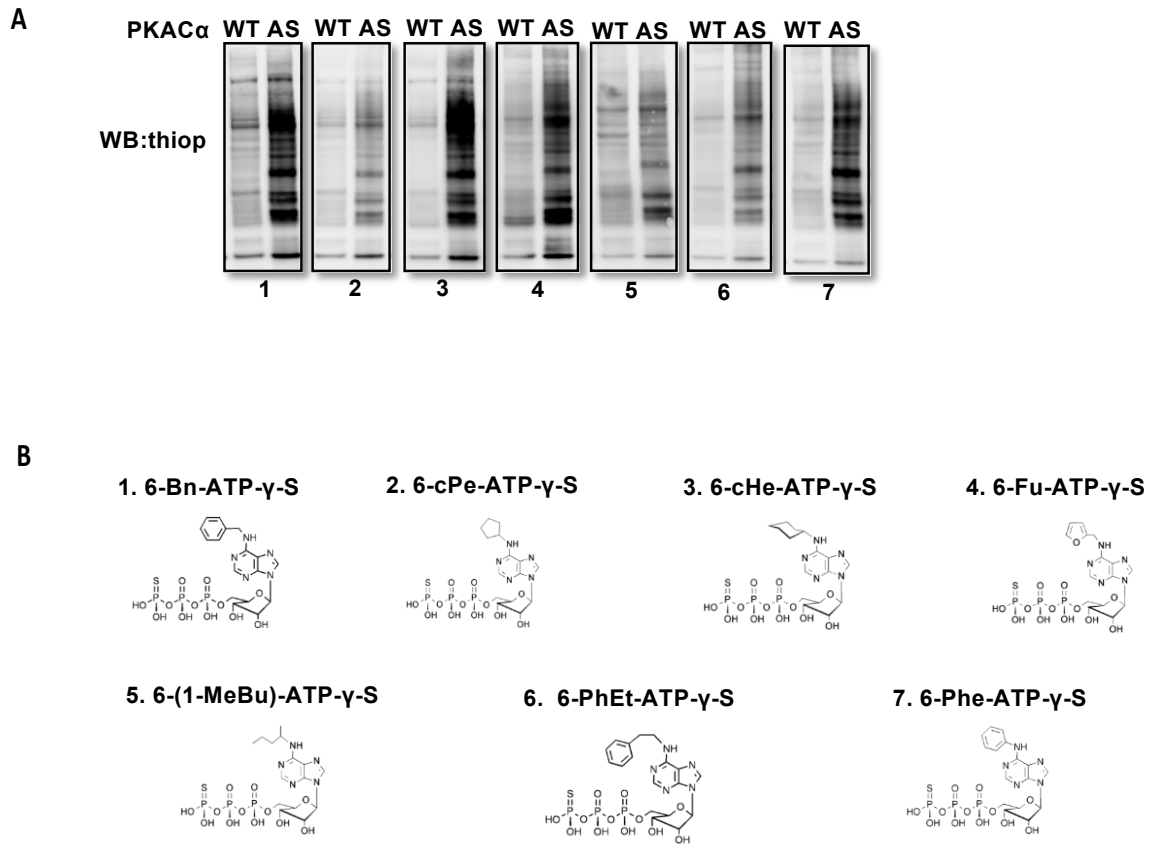

Figure S1. Screen for the best N6-substituted ATPgS analog as a phosphodonor of AS-PKACα **(A)**Kinase assay in HUVEC lysates using WT-PKACα and AS-PKACα. All the western blot membranes exposed at the same time. **(B)**Structural formulas of 7 different N6-substituted ATPgS analogs.

Figure S2

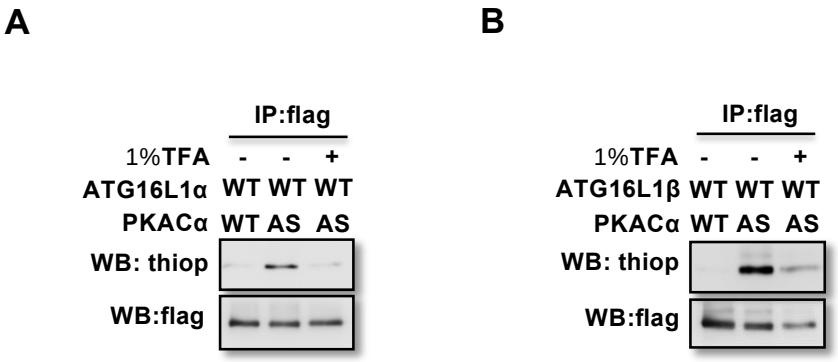

Figure S2. Thiophophorylation is converted to normal phosphoryation by 1% TFA acid–promoted hydrolysis. (A-B)ATG16L1a(A) and ATG16L1β(B) thiophosphorylated and immunoprecopitated as in Figure 1C, then treated with or without 1% TFA at 37 °C for 4 hours.

Figure S3

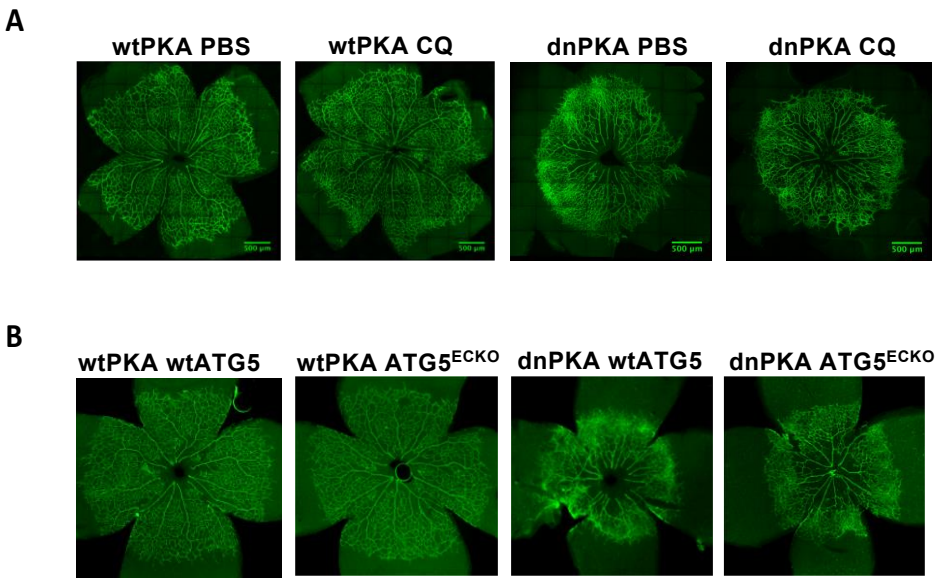

Figure S3. Whole retina imagines of autophagy inhibition partially rescues retinal vascular hypersprouting caused by PKA deficiency. (A) wtPKA and dnPKA^{iEC} mice treated with PBS or CQ were injected with tamoxifen from P1 to P3, then retinas were collected at P6. Vasculature was visualized with isolectin B4-Alexa Fluor 488. **(B)** wtPKA with wtATG5 or ATG5^{ECKO} mice and dnPKA^{iEC} with wtATG5 or ATG5^{ECKO} mice were injected with tamoxifen from P1 to P3, then retinas were collected at P6. Vasculature was visualized with isolectin B4-Alexa Fluor 488.